Solar irradiance reduction via climate engineering: Impact of different techniques on the energy balance and the hydrological cycle

U. Niemeier,[1] H. Schmidt,[1] K. Alterskjær,[2] and J. E. Kristjánsson[2]

[1] Different techniques of solar radiation management (SRM) have been suggested to counteract global warming, among them the injection of sulfur into the stratosphere, mirrors in space, and marine cloud brightening through artificial emissions of sea salt. This study focuses on to what extent climate impacts of these three methods would be different. We present results from simulations with an Earth system model where the forcing from the increase of greenhouse gases in a transient scenario (RCP4.5) was balanced over 50 years by SRM. While global mean temperature increases slightly due to the inertia of the climate system and evolves similar with time for the different SRM methods, responses of global mean precipitation differ considerably among the methods. The hydrological sensitivity is decreased by SRM, most prominently for aerosol-based techniques, sea salt emissions, and injection of sulfate into the stratosphere. Reasons for these differences are discussed through an analysis of the surface energy budget. Furthermore, effects on large-scale tropical dynamics and on regional climate are discussed.

1. Introduction

[2] Within the ongoing debate on anthropogenic climate change, the suggestion of a deliberate manipulation of climate has gained some attention. Such climate engineering (CE) techniques, also named geoengineering, are usually divided into two major groups: carbon dioxide removal and solar radiation management (SRM). SRM refers to the artificial reduction of the amount of solar radiation reaching the surface of the Earth. Techniques suggested to reach this goal include injections of sulfur into the stratosphere to form aerosol particles and mimic the effect of large volcanic eruptions [e.g., *Budyko*, 1977; *Crutzen*, 2006], mirrors in space [e.g., *Mautner*, 1991], and the brightening of marine clouds by emission of sea salt aerosols acting as cloud condensation nuclei [e.g., *Latham*, 1990]. An overview of methods and an attempt to quantify their cooling potential is provided by *Lenton and Vaughan* [2009]. In this study, we will compare different SRM techniques with respect to their effects on climate and in particular on the hydrological cycle.

[3] Radiative forcing caused by greenhouse gases differs from CE forcing in spatial and temporal distribution.

Therefore, an engineered climate would globally and regionally differ from a naturally balanced climate of the same global mean temperature [e.g., *Govindasamy and Caldeira*, 2000; *Schmidt et al.*, 2012]. Simulated responses to SRM show some robust characteristics, e.g., reduction of pole-to-equator temperature gradient and a decrease in global mean precipitation [*Bala et al.*, 2008; *Schmidt et al.*, 2012; *Irvine et al.*, 2011]. However, in many details, for instance regional precipitation patterns, the responses differ among models, even if the same SRM method is applied. To better understand potential climate effects of SRM and to identify robust response patterns, a set of numerical SRM experiments [*Kravitz et al.*, 2011a] was defined within the Geoengineering Model Intercomparison Project (GeoMIP). The intercomparison of the GeoMIP experiment G1 (an instantaneous compensation of a quadrupling of the CO_2 concentration) confirmed the abovementioned robust characteristics but also enabled a quantification of the uncertainty of response estimates and to better identify regional response patterns [*Schmidt et al.*, 2012; *Kravitz et al.*, 2013b; *Tilmes et al.*, 2013].

[4] As in the abovementioned GeoMIP case, most other numerical studies have concentrated on single SRM techniques [*Jones et al.*, 2010, 2009; *Rasch et al.*, 2008], in some cases comparing different applications, e.g., global versus regional SRM forcing [*Caldeira and Wood*, 2012; *Robock et al.*, 2008; *Ricke et al.*, 2010]. Only few studies show the impact of different SRM techniques [*Jones et al.*, 2011; *Ammann et al.*, 2010], but their studies were not

[1]Max Planck Institute for Meteorology, Hamburg, Germany.
[2]Department of Geosciences, Meteorology and Oceanography Section, University of Oslo, Oslo, Norway.

Corresponding author: U. Niemeier, Max Planck Institute for Meteorology, Bundesstr 53, 20146 Hamburg, Germany. (ulrike.niemeier@zmaw.de)

Table 1. Scenarios Used in This Study

Scenario	Description	Area of Implementation
RCP4.5	CMIP5 scenario; 4.5 W/m^2 radiative GHG forcing in 2100.	
SOL	Mirrors at the Lagrangian point.	Global
SULF	Injection of sulfate into the stratosphere.	Global
SALT	Emission of sea salt aerosol over the ocean to brighten marine stratocumulus clouds and increase reflection from sea salt particles in clear sky.	30°N to 30°S
FIX	Anthropogenic forcing kept frozen at the 2020-level.	Global
RCP2020	Average over year 2016 to 2025 of RCP4.5.	
RCP2065	Average over year 2060 to 2069 of RCP4.5.	
CE2065	Average over year 2060 to 2069 of SRM scenarios.	

designed for a direct comparison of the impacts of different SRM techniques.

[5] This study with a state-of-the-art Earth system model (ESM) is based on the GeoMIP G3 scenario, where the increase of anthropogenic greenhouse gases (GHG) after year 2020 is balanced to keep the radiative forcing constant. The increase of GHG is assumed to follow the RCP4.5 scenario as defined in the fifth phase of the Climate Model Intercomparison Project (CMIP5) [*Taylor et al.*, 2012] protocol. We employ three different SRM techniques: injection of sulfate into the stratosphere (SULF), mirrors in space (SOL), and artificial emissions of sea salt over the oceans (SALT) (Table 1). The main question this study intends to answer is to what extent these three methods would produce different climates. A global mean reduction of precipitation, e.g., has been discussed as a response to aerosols from both pollution and volcanic eruptions [e.g., *Liepert and Previdi*, 2009; *Trenberth and Dai*, 2007] as well as to SRM in general [*Bala et al.*, 2008]. To our knowledge, it has, however, not been studied to what extent the response depends on the specific technique of SRM.

[6] Our study is organized as follows: In section 2, the model and a description of the simulated scenarios are presented. In section 3, we present and discuss the responses of global mean climate parameters to the different SRM techniques with a focus on the hydrological cycle and the surface energy budget. Section 4 presents differences in the regional responses to the SRM techniques.

2. Experimental Description

2.1. Model Description

[7] The simulations have been performed with the Max-Planck-Institute's Earth system model (MPI ESM) [*Giorgetta et al.*, 2013]. The model is a state-of-the-art coupled three-dimensional atmosphere-ocean-land surface model, with a well-represented stratosphere and an interactive carbon cycle. It consists of the atmosphere component ECHAM6 [*Stevens et al.*, 2013], and the ocean component Max Planck Institute Ocean Model (MPIOM) [*Jungclaus et al.*, 2013] includes submodels for land processes (JSBACH) [*Reick et al.*, 2013], vegetation, and ocean biogeochemistry. ECHAM6 was used in T63 spectral resolution (1.8°) with 47 vertical levels and a center of the model top layer at 0.01 hPa. MPIOM applies a conformal mapping grid of about 1.5°. Ocean and atmosphere are coupled daily without flux corrections. With this model version,

a number of simulations have been performed following the CMIP5 protocol.

2.2. Description of Scenarios

[8] GeoMIP proposed a set of numerical experiments in which the climate forcing, as defined in experiments of the CMIP5 protocol, is balanced via SRM [*Kravitz et al.*, 2011a]. This study follows GeoMIP experiment G3, an experiment parallel to CMIP5 experiment RCP4.5, assuming transient increase of anthropogenic forcing up to 4.5 W/m^2 in 2100. Within G3 using stratospheric aerosols, the radiative forcing of anthropogenic GHGs should be balanced to maintain the net radiative forcing at the top of the atmosphere (TOA) close to the one of 2020. The mean deviation from 2020 values is requested to be below 0.1 W/m^2. The exact simulated anthropogenic forcing in RCP4.5 depends on the climate model, and the time dependence is difficult to assess. However, in GeoMIP, it was agreed to balance an estimated forcing as tabulated in the CMIP5 protocol.

[9] To study the impact of different SRM methods on climate, we performed not only the original GeoMIP G3 simulation which will be called SULF in the following but also simulations where the same compensation of forcing is realized through other SRM techniques (Table 1): mirrors at the Lagrangian point (SOL), and emission of sea salt aerosol over the ocean to brighten marine stratocumulus clouds and increase reflection from sea salt particles in clear sky (SALT).

[10] We compare the simulated SRM climate of the last decade (2060–2069) of a 50 year simulation, starting in 2020, to the 10 year mean around the year 2020, taken as an average over the years 2016 to 2025 of the RCP4.5 simulation (RCP2020). In a control experiment, we kept the anthropogenic forcing frozen at the 2020-level (FIX). Therefore, FIX can also be interpreted as resulting from a mitigation strategy, or carbon dioxide removal. This experiment allows us to assess how well the GHG radiative forcing in the SRM experiment is balanced and finally to correct for potential imbalances (see section 2.3). Although radiative forcings are kept frozen in this experiment, due to the inertia of the climate system the global mean temperature still increases by about 0.3 K over the 50 years until 2069, as further discussed in section 3.1.

[11] For each scenario, an ensemble of three members has been calculated. All presented results are ensemble averages.

2.2.1. Mirrors at the Lagrangian Point (SOL)

[12] Mirrors in space are represented in the model via a reduction of the total solar irradiance (S_0) which is applied
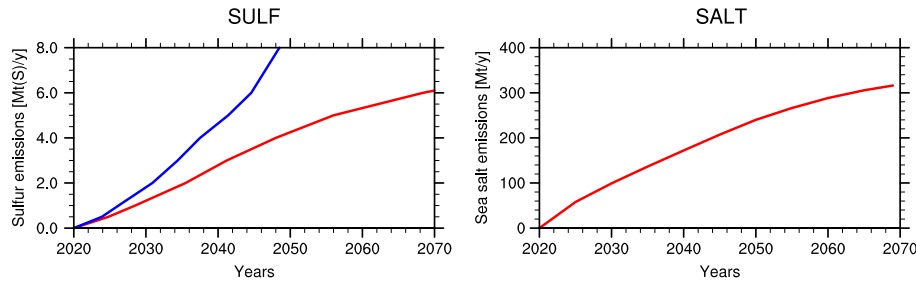
Figure 1. Emissions (left) of sulfur into the stratosphere and (right) of sea salt into the marine boundary layer between 30°S and 30°N necessary to balance GHG forcing of RCP4.5 (red) and RCP8.5 (blue; not used in this study).

homogeneously across the solar spectrum. According to the experiment specifications by *Kravitz et al.* [2011b] in the idealized experiment G1, a quadrupling of CO_2 with forcing (F_{4CO2}) was compensated by a reduction δS_0, estimated as $\delta S_0 = -4F_{4CO2}/(1 - \alpha)$ to account for the sphericity of Earth and planetary albedo α. Balancing RCP4.5, instead of F_{4CO2}, the difference of forcing to the start year 2020 has been taken into account, as well as the efficacy of forcing from total solar irradiance with respect to that from CO_2 as calculated from G1 [*Schmidt et al.*, 2012]. The process to balance a given anthropogenic forcing via the reduction of S_0 is described in detail for a constant forcing in *Schmidt et al.* [2012] and *Kravitz et al.* [2011a].

2.2.2. Injection of Sulfur Into the Stratosphere (SULF)

[13] The MPI-ESM does not calculate the evolution of aerosols explicitly. Aerosol effects on radiation need to be prescribed in terms of their optical properties. In the MPI-ESM, these properties are calculated based on aerosol optical depth (AOD) at 0.55 nm and the effective radius. These parameters were precalculated using the aerosol microphysical model HAM [*Stier et al.*, 2005] coupled to the general circulation model MAECHAM5 [*Giorgetta et al.*, 2006] as it has been done earlier for studies of volcanic eruptions [*Timmreck et al.*, 2010]. Simulations for emission rates of 0.5, 2, 4, 6, and 8 Mt(S)/y were performed as described in detail by *Niemeier et al.* [2011]. In these simulations, SO_2 was injected into an 1.8° × 1.8° area close to the equator at a height of 60 hPa.

[14] The radiative forcing resulting from the different emission rates was diagnosed in several short preparatory simulations with the MPI-ESM using a double call of the radiation, one with aerosols and one without. Figure 1 (left) shows the amount of sulfur emissions needed in the MPI-ESM to compensate the post-2020 forcings under RCP4.5 and RCP8.5.

2.2.3. Sea Salt Injections: A Direct Radiative Effect and Brightening of Marine Clouds (SALT)

[15] The emission of sea salt over the oceans is supposed to increase the reflectivity of marine stratocumulus clouds. The injection of sea salt increases the cloud droplet number concentration (CDNC), through the indirect aerosol effect [*Twomey*, 1977]. Under high CDNC, clouds contain more, but smaller, droplets which increase the total surface area of droplets and therefore the cloud albedo. The decrease in droplet size may reduce the amount of warm rain through affecting the autoconversion [*Albrecht*, 1989] and therefore increase the cloud albedo through increasing the cloud liquid water path. Sea salt is also injected over cloud-free areas,

where the sea salt particles enhance reflection of short wave radiation (direct effect).

[16] The MPI-ESM is not capable of explicitly calculating the evolution of sea salt aerosols and their interaction with clouds. Similar to SULF, the direct effect is implemented through prescribed fields of aerosol optical properties, the indirect effect by adding a precalculated cloud droplet number concentration (CDNC) to the CDNC over oceans within the MPI-ESM. In the MPI-ESM, we estimated the forcing resulting from sea salt optical properties and CDNC using the method of *Gregory et al.* [2004]. As this method does not provide accurate results for small forcings, we have additionally used a double radiation call which, however, can only account for the direct aerosol effect. The forcing compensation required for every simulated year is shown in Figure 1 (right).

[17] The microphysical evolution of sea salt emissions and distribution of particles was simulated with the Norwegian ESM (NorESM) [*Bentsen et al.*, 2013]. This model includes a prognostic treatment of both sea salt [*Struthers et al.*, 2011] and cloud droplet number concentration. The injections of sea salt with a mean dry modal radius of 0.13 µm were uniform and confined over the oceans between 30°N and 30°S (K. Alterskjær et al., The transient response in three Earth system models to a cancellation of 21st century RCP4.5 forcing through sea salt injections into the low-latitude marine boundary layer, submitted to *Journal of Geophysical Research*, 2013) based on a study of *Alterskjær et al.* [2012]. They were not considered to depend on the wind speed.

[18] An earlier study [*Partanen et al.*, 2012] has already indicated that the direct effect of additionally emitted sea salt on radiation may not be negligible, when emitting sea salt over large parts of the ocean. There, the ratio of radiative forcing caused by the direct effect versus the indirect effect is 2:3. It should be noted that both MPI-ESM and NorESM show a stronger direct than indirect effect of the sea salt aerosols.

2.2.4. Surface Short Wave Radiation Anomalies

[19] Figure 2 shows the clear-sky net short wave (SW) radiation anomaly at the surface, which, to a large extent, reflects the applied forcing. Besides the changes from SRM, also changes in water vapor and land use (tropics and midlatitudes) show a clear signal in SW radiation. In all scenarios, clear-sky SW fluxes increase toward the North Pole. This response is mainly due to increased temperatures and therefore reduced sea ice and snow cover during the spring season. Additionally, the applied methods are more effective
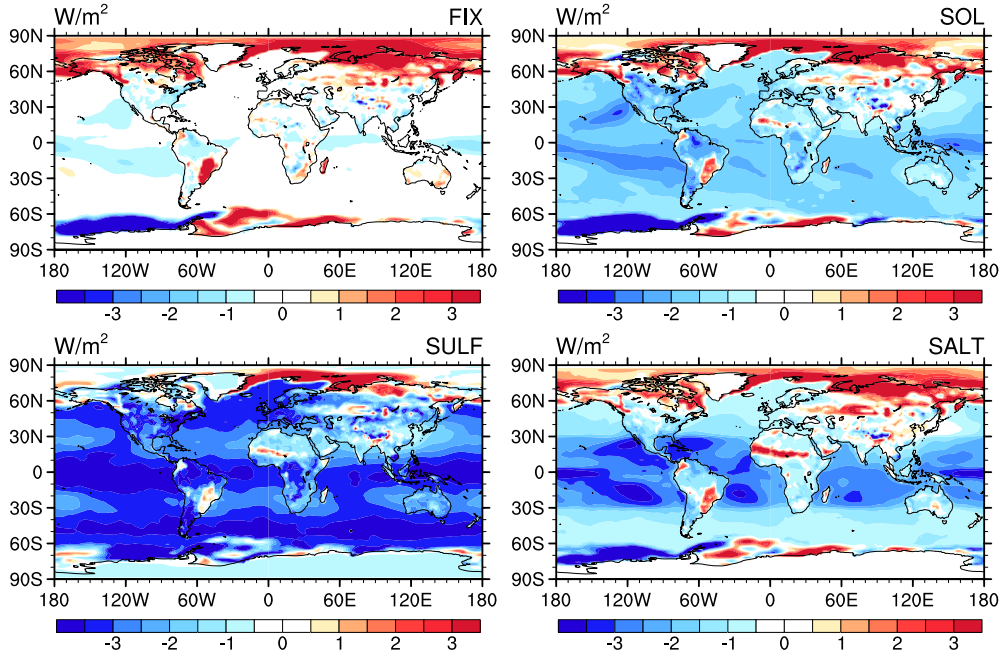
Figure 2. SW surface flux anomalies for clear-sky conditions. Anomalies are presented as differences between the engineered states CE2065 and the reference climate RCP2020. For SALT only, the direct effect of sea salt is included in this figure, not the indirect effect, as cloud effects are excluded under clear-sky conditions.

at low solar zenith angles and in regions of low albedo [*Bala et al.*, 2008].

[20] From the globally acting SRM in experiment SOL, an almost global decrease of net downward SW radiation is resulting. Local minima and maxima in SW surface radiation in experiment SULF follow closely the zonal distribution of AOD of sulfate [*Niemeier et al.*, 2011], which has maxima in the tropics and midlatitudes. Reflection of SW radiation by sulfate aerosols is especially effective in spring close to the poles, as a consequence of transport via the Brewer-Dobson circulation.

[21] Sea salt is emitted in experiment SALT between 30°N and 30°S but a small fraction of the sea salt aerosols is also transported toward higher latitudes. Clear-sky SW radiation is representing the direct effect of the aerosols only. The impact of the indirect cloud effect, brightening of the clouds as well as increased cloud cover, decreases the SW surface radiation within the seeding area by an additional 1 to 2 W/m².

2.3. Bias Correction to Enable Comparison of the SRM Methods

[22] The SRM strategy in our experiments was to compensate the additional climate forcing in the RCP4.5 scenario after 2020 by different methods. However, the compensation is necessarily imperfect, as both the greenhouse gas forcing and the forcing from the specific SRM technique are not known exactly. Hence, differences between climate states may be influenced by an imperfect compensation of the forcing. To allow for a comparison, results of the CE experiments need to be bias corrected. We perform this correction in relation to experiment FIX. With its frozen GHG concentrations, FIX can be seen as an analog for a perfect compensation of the forcing through the GHG increase after

2020 and is unbiased by construction. We have calculated for every SRM experiment $i \in$ {SULF, SALT, and SOL} a correction factor

$$\alpha_i = \frac{<I_i(t)> - <I_{\text{FIX}}(t)>}{<I_{\text{RCP4.5}}(t)> - <I_{\text{FIX}}(t)>}, \quad (1)$$

where $I_i(t)$ is a yearly mean of the total radiative net flux imbalance at TOA in experiment i and the angle brackets denote the time mean over the years 2020 to 2069. I_{FIX} and $I_{\text{RCP4.5}}$ are the respective values of experiment FIX and RCP4.5. The denominator is the time average additional forcing of scenario RCP4.5 after 2020 that needs to be compensated. For a perfect compensation, $<I_i(t)>$ would be equal to $<I_{\text{FIX}}(t)>$. The calculated correction factors for the SRM experiments are the following:

$$\alpha_{\text{SULF}} = -0.080 \quad (2)$$
$$\alpha_{\text{SOL}} = 0.141 \quad (3)$$
$$\alpha_{\text{SALT}} = 0.011, \quad (4)$$

indicating that the maximum deviation from perfect compensation occurs in the SOL case with an underestimation of the necessary compensation by about 14%.

Annual mean state variables $\chi_i(t)$ of experiment i at year t are then corrected by

$$\chi_i'(t) = \chi_i(t) - \alpha_i[\chi_{\text{RCP4.5}}(t) - \chi_{\text{FIX}}(t)], \quad (5)$$

i.e., it is assumed that the influence of the compensation bias on any state variable increases linearly with the increasing deviation of the respective state variables in simulations RCP4.5 and FIX. The bias correction is defined in a way ensuring that the bias of the total radiative net flux imbalance at TOA would be corrected perfectly:
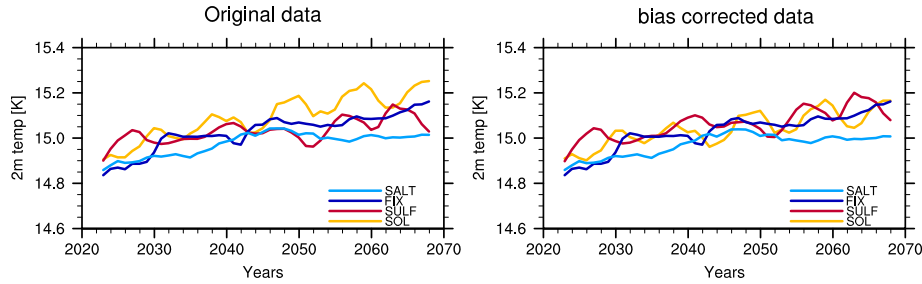
$$<I_i'> = <I_{\text{FIX}}>. \quad (6)$$

Figure 3. Global and yearly mean 2 m temperatures as (left) originally simulated and (right) after bias correction.

We applied the correction to annual mean 2 m temperatures, evaporation, precipitation, and energy fluxes at the surface and TOA. Figure 3 compares the originally simulated and the bias-corrected temperatures.

[23] Another option would be to bias correct for the difference of global mean temperature to experiment FIX instead of TOA imbalance. However, as the protocol for experiment G3 demands to aim for a compensation of the TOA forcing, we opted for this parameter. Tests have indicated that correcting for temperature instead would not alter our main results.

3. The Dependence of Global Mean Precipitation on the SRM Method

[24] Earlier studies have shown that SRM, in general, leads to a reduction of precipitation that would overcompensate the long-term increase of precipitation caused by the temperature increase due to GHG forcing of opposite sign (see section 1). An interesting result of the simulations, presented here as global mean data, is that the response of the hydrological cycle differs among the different SRM methods. In this section, we discuss these differences mainly as comparison between CE2065 and RCP2020. First, the time evolution of global mean variables is described (section 3.1), followed by some basic considerations on the surface energy budget (section 3.2), and by a discussion of these budgets in the different simulations (section 3.3). All results are corrected to account for forcing differences as discussed above.

3.1. Temporal Evolution of Global Mean Data

[25] In our experiments, SRM is applied starting in year 2020 from a transient RCP4.5 simulation. Figure 4 shows the temporal evolution of 5 year running mean global 2 m temperature, net SW surface radiation, and evaporation for the different experiments. When starting from a transient simulation, due to the inertia of the climate system, the model is not in an equilibrium state and still has to adapt to the residual forcing. Therefore, the control simulation (FIX) with constant 2020 forcing still shows a trend: TOA energy imbalance is decreasing (not shown) along with an increase of 2 m temperature (Figure 4a). The temperature in the SRM experiments follows this trend; only SALT shows, despite neither TOA nor surface energy balance differ significantly from the other experiments, overall slightly lower temperatures. The reason for this is not yet understood. Net all-sky SW radiation at the surface (Figure 4b) is stable in time for FIX. For all SRM experiments, surface all-sky SW radia-

tion is decreasing as well as evaporation, with precipitation following the same trend.

[26] While global mean temperature evolves very similarly with time for the different SRM scenarios, the responses of net SW surface flux and global mean evaporation differ considerably (see Figures 4b and 4c). *Bala et al.* [2008] discuss the precipitation response for a case where a CO_2 increase is compensated by a reduction of solar irradiance and argue that the solar forcing acts more on the surface, while CO_2 forcing is mainly longwave (LW) forcing which impacts the entire troposphere. Additionally, a CO_2 increase without increasing temperature, e.g., in the very early phase of a simulation with an abrupt 4 times CO_2 increase, decreases precipitation [*Andrews et al.*, 2009] as a consequence of the loss of LW radiation to space [*Bony et al.*, 2013] and the stabilization of the troposphere. This direct response is mainly responsible for the reduction in precipitation rate by the forcing agent CO_2 [*Andrews et al.*, 2009] and important in our experiments, as the temperature change is small. In typical numerical SRM experiments, the zero temperature change under enhanced CO_2 has been realized through reduction of the solar constant and has been shown to result in a reduction in precipitation [e.g., *Govindasamy and Caldeira*, 2000; *Schmidt et al.*, 2012]. It can explain, why global mean evaporation at the end of experiment SOL is lower than at the end of experiment FIX (Figure 4c). Precipitation is further reduced for the aerosol scenarios SALT and SULF. Reduction of precipitation has been discussed for aerosols from pollution [e.g., *Rosenfeld et al.*, 2008; *Liepert and Previdi*, 2009] and volcanic eruptions [e.g., *Trenberth and Dai*, 2007]. In the following, we will attempt to explain, why the global mean precipitation is even further reduced, when SRM is realized by sulfate aerosols or sea salt instead of a reduction of the incoming solar irradiance at the TOA.

3.2. Comparing Energy Budgets for Transient Climate States

[27] *Andrews et al.* [2009] show that differences between the radiative forcings at TOA and surface are compensated by condensational heating changes in the troposphere that are related to changes in surface latent heat fluxes (LH) and precipitation rates. This can explain initial fast responses of the hydrological cycle to forcings like, e.g., abrupt doubling of the CO_2 concentration [*Andrews et al.*, 2009]. B. Kravitz et al. (An energetic perspective on hydrologic cycle changes in the Geoengineering Model Intercomparison Project (GeoMIP), submitted to *Journal of Geophysical Research*, 2013a) use this concept to discuss precipitation
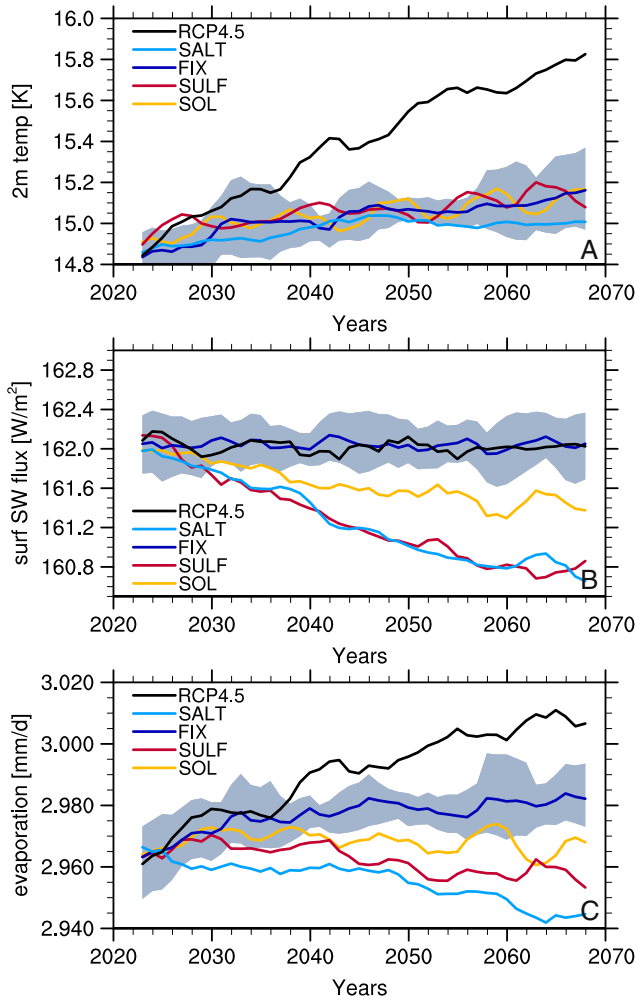
Figure 4. Globally and temporally averaged ensemble mean time series (running mean over 5 years) of the SRM experiments and RCP4.5 experiment. (a) The 2 m temperature (K), (b) net surface SW radiation (all-sky; W/m²), and (c) evaporation (mm/d). The gray shading shows the minimum and maximum values of the yearly mean of the single ensemble members for FIX. The ensemble span in the other experiments is similar to the one in FIX but omitted for clarity of the presentation. Fluxes are defined positive downward.

responses in the GeoMIP G1 experiment, where an abrupt quadrupling of CO_2 is balanced via a change of solar irradiance, similar to SOL. In a transient simulation as used in this study, the situation is more complicated as forcing and response evolve together.

[28] *Liepert and Previdi* [2009] discuss differences in observed and modeled precipitation response to global warming under transient conditions. They link changes in precipitation and according changes in latent heat flux (ΔLH) to changes in surface energy fluxes:

$$L\Delta P = -\Delta\text{LH} = \Delta R_{\text{SRF}} + \Delta\text{SH} - \Delta M, \tag{7}$$

where ΔP is the precipitation change, L is a constant representing the energy of phase transition, ΔR_{SRF} is the change in total surface radiative fluxes (SW + LW), ΔSH is the change

in sensible heat flux, and ΔM is the change in ocean and land heat uptake. In our case, the changes Δ are the differences between the climate states of the CE2065 and RCP2020.

[29] Following the assumption that on decadal time scales, ocean and land heat uptake is equal to TOA radiative imbalance [*Hansen et al.*, 2005; *Liepert and Previdi*, 2009]:

$$L\Delta P = \Delta R_{\text{SRF}} - \Delta R_{\text{TOA}} + \Delta\text{SH}. \tag{8}$$

As in our model, in general, global changes in latent heat flux dominate changes in sensible heat flux, and thus, ΔP is approximately linearly related to the difference of radiative imbalances at the surface and TOA. Table 2 shows this for the results of equation (8) in comparison to model results of precipitation.

[30] Our main goal is, however, not to compare the states CE2065 and RCP2020 in single experiments, but the responses of the different SRM methods. As by design ΔR_{TOA} is approximately equal in all experiments, one can explain differences in the precipitation responses by differences in surface flux changes only. Furthermore, as to a good approximation, responses to forcings can be considered independent of the forcing mechanism [*Hansen et al.*, 1997]; one can relate the different surface flux changes to differences in the surface forcings caused by the SRM methods.

3.3. The Impact of the SRM Method on the Energy Budget

[31] The basic idea of the three studied SRM methods is the installation of a layer reflecting SW radiation in or above the atmosphere to keep the TOA radiative forcing at year 2020 levels. Before analyzing effects of the specific methods, it is useful to qualitatively discuss the dependence of the surface energy budget on properties of such a reflector:

[32] 1. A reflecting layer that has a greenhouse effect in addition to its reflecting properties reduces precipitation stronger than one that has reflecting properties only. The positive temperature response to a greenhouse effect needs to be compensated by a stronger reflector and hence causes a stronger effect on surface SW radiation. This causes a stronger precipitation effect than the change in LW radiation related to the greenhouse effect.

[33] 2. The ratio of surface to TOA net SW forcing resulting from a reflecting layer decreases with increasing altitude of the layer. The SW surface forcing, and thereby also the effect on precipitation, for a given TOA SW forcing, is larger the lower down in the atmosphere the layer is installed. This

Table 2. Changes in Global Mean Net Radiative Fluxes at TOA (R_{TOA}) and Surface (R_{SRF}), i.e., the atmospheric heating imbalance, and the product of global mean annual precipitation ΔP and energy of phase transition ($L = 2.5$ MJ/kg) following equation (8) (P_{eq}) and calculated from the model experiments (P_{exp})[a]

Scenario	$\Delta(R_{\text{SRF}} - R_{\text{TOA}})$	$L\Delta P_{\text{eq}}$	$L\Delta P_{\text{exp}}$
Unit	(W/m²)	(W/m²)	(W/m²)
SALT	−0.75	−0.69	−0.65
SULF	−0.38	−0.24	−0.25
SOL	−0.01	0.03	−0.01
FIX	0.48	0.42	0.41

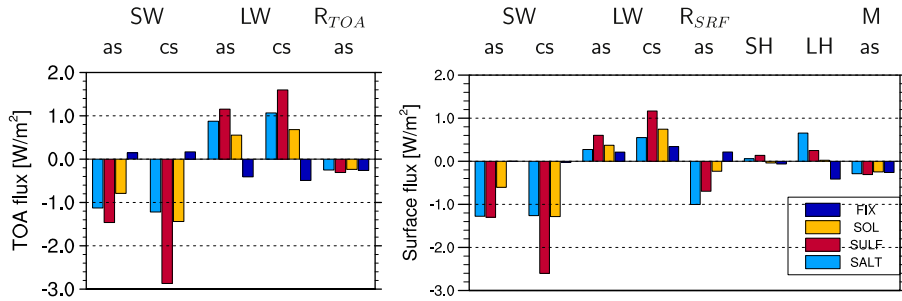[a]Values are presented as differences between CE2065 and RCP2020.

Figure 5. Global mean energy flux differences (W/m^2) at (left) the top of the atmosphere and (right) the surface between CE2065 and RCP2020 for all-sky (as) and clear-sky (cs) conditions. SW: shortwave radiation, LW: longwave radiation, R_{TOA}: total (LW+SW) radiation at TOA, R_{SRF}: total radiation at the surface, SH: sensible heat flux, LH: latent heat flux, M: heat uptake. Fluxes are defined positive downward.

is related to radiative transfer through the atmosphere by the absorbing and reflecting properties. Of a, say, 1 W/m^2 TOA forcing from SW reflection near the TOA only a part arrives at the surface, because of absorption and reflection of downward radiation by the atmosphere itself. On the other hand, a 1 W/m^2 additional reflection near the surface causes a smaller TOA SW forcing due to absorption and downward reflection of the upward beam.

[34] Figure 5 shows the parameters of the global energy budget at (left) TOA and (right) surface for differences between CE2065 and RCP2020 states for all-sky (as) and clear-sky (cs) conditions. Clear-sky fluxes are calculated without considering radiative effects of clouds.

[35] FIX: In the case of fixed 2020 forcing, $\Delta \text{LW}_{\text{TOA}}$ is weakly negative. This increase in outgoing LW radiation results from the increasing global temperature. The net SW radiation partly compensates the LW change, probably due to surface feedbacks, related mainly to ice and snow cover. Changes in cloud effects are negligible. At the surface, small positive changes of LW_{SRF} are probably related to the greenhouse effect of the increased water vapor content. According to equation (8), the different changes of TOA and surface net downward radiation are compensated by an increase of the upward directed latent heat flux and thereby mainly responsible for the simulated increase in precipitation in FIX.

[36] SOL: In simulation SOL, $\Delta \text{LW}_{\text{TOA}}$ is positive as a consequence of the increased CO_2 concentration, while the reduction of total solar irradiance is resulting in a decrease of $\Delta \text{SW}_{\text{TOA}}$. This latter effect is larger in the clear-sky analysis than for all-sky conditions, which is partly related to the negative feedback of a decreased low cloud cover described by *Schmidt et al.* [2012] as a robust feature of equilibrium simulations. Additionally, even without changed clouds, changes in clear sky would be larger than in all-sky SW flux because of the high cloud albedo. The difference of TOA and surface net radiative fluxes is small, and so are ΔLH and precipitation change. In comparison to experiment FIX, however, precipitation is lower. The reason is related to the decrease in SW surface radiation and the additional impact of CO_2 [*Bony et al.*, 2013] as discussed in section 3.1.

[37] SULF: In comparison to SOL, in SULF, the changes of SW_{TOA} and LW_{TOA} are larger. Sulfate aerosols do not only scatter shortwave radiation, but they additionally absorb near infrared and longer wavelengths [*Lohmann and*

Feichter, 2005]. This greenhouse effect requires a further decrease in the SW surface flux as discussed above and causes the, in comparison to SOL, reduced precipitation. It is interesting to note that sulfate aerosols have a strong cloud effect on shortwave radiation of more than 1 W/m^2 at both surface and TOA, which is similar to the SW cloud effect in SOL.

[38] SALT: On the first glance, differences between SOL and SALT at TOA seem small. The additional LW clear-sky flux difference for SALT results from sea salt aerosols also having a greenhouse effect besides their scattering properties [*Li et al.*, 2008] which is smaller than in SULF. A difference between SALT on the one hand and SOL and SULF on the other hand is that for SALT, the negative clear-sky SW surface forcing is about equal to the TOA forcing while it is slightly smaller than the TOA forcing in the other two cases. This is likely related to the different altitudes at which the reflector is installed as discussed above.

[39] The cloud brightening is just compensating for the overall decrease of cloud fraction under SRM, which can be seen from clear-sky and all-sky forcings to be very similar. However, Figure 5 shows that the response of latent heat flux is strongly dominating only in SALT. This is most likely due to the sea salt aerosols being emitted over the oceans, while sulfate aerosols act over land and oceans. Over dry land regions a change in surface radiation flux can less easily be compensated by a change in evaporation than over the oceans. So we assume that the stronger change in atmospheric heating is caused by influencing cloud physics and changes in latent heat.

[40] The energy balance cannot explain the lower global temperature in SALT. This is most probably related to cloud-radiation interactions in the lower troposphere and cannot be answered with this analysis of the energy budget. The temperature difference between experiments SALT and SULF impacts the precipitation. If the bias correction was performed with respect to global temperature and not TOA fluxes (see section 2.3), the difference in precipitation between these two experiments would be smaller.

4. The Dependence of Precipitation Patterns on the SRM Method

[41] It has been shown in the previous sections that some aspects of the globally averaged energy budget respond
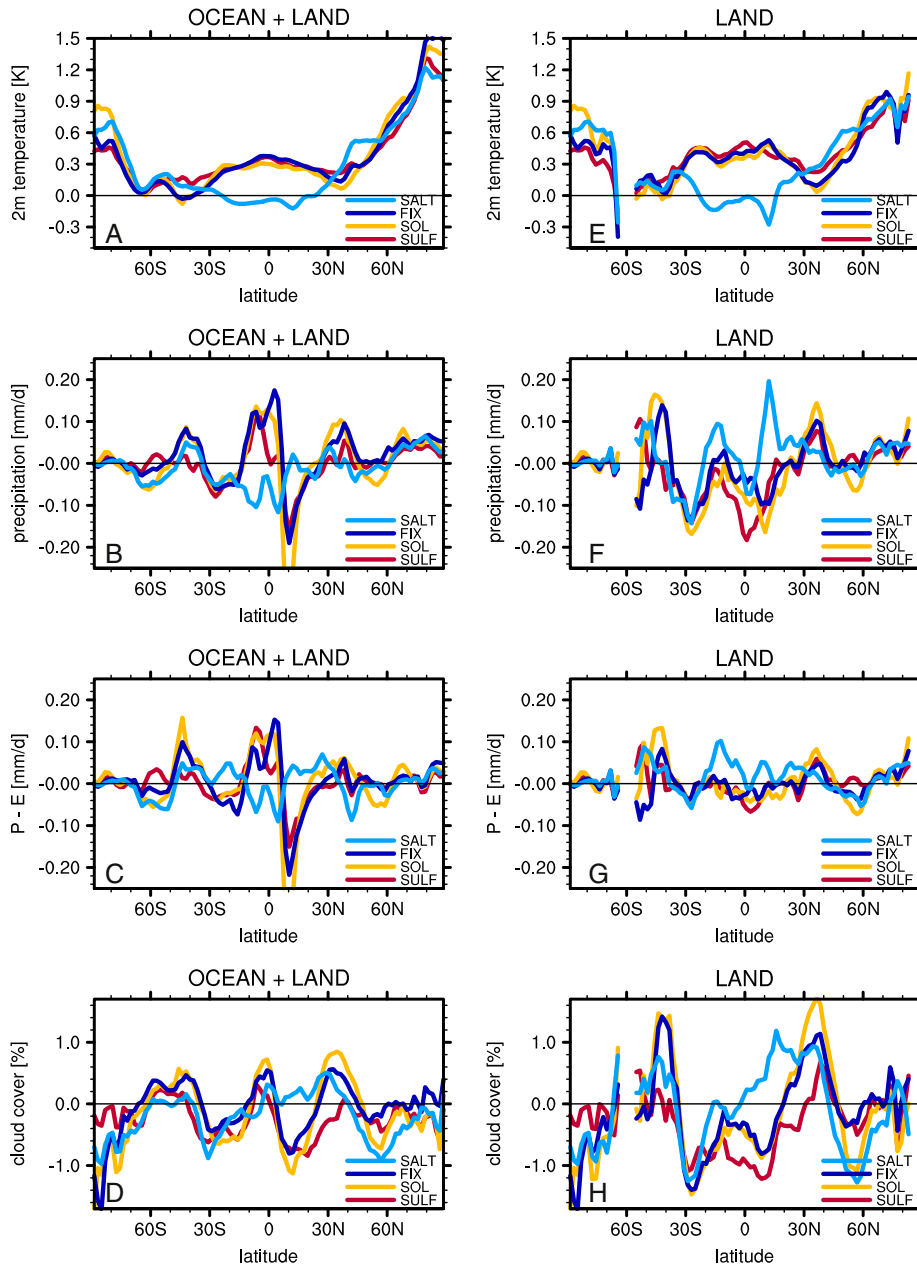
Figure 6. Zonal mean anomalies of 2 m temperature, precipitation, precipitation minus evaporation, and cloud cover calculated (a–d) over all surfaces and (e–h) over land surfaces only. Anomalies are presented as differences between the engineered states CE2065 and the reference climate RCP2020.

differently to various CE methods. However, ecosystems react to changes on regional scales, and one may expect even stronger regional than global differences among the methods as the SRM techniques do not act homogeneously over the globe. Therefore, in this section, we describe zonal mean SRM impacts on temperature and precipitation (4.1), as well as the impact on large scale dynamics and precipitation patterns (4.2). All results are presented as differences between the engineered climate CE2065 and the reference RCP2020.

4.1. Zonal Mean Temperature, Clouds, and Precipitation

[42] Figures 6a–6d show zonal mean responses of temperature, precipitation, precipitation minus evaporation, and

total cloud cover in the different experiments. Responses in experiments FIX, SOL, and SULF are generally similar to each other, while the response patterns in SALT differ in the seeding region between 0°S and 30°N. This indicates that the responses to SULF and SOL are largely determined by the residual temperature increase, while SALT causes a distinct SRM pattern in that region.

[43] The residual increase of temperature from RCP2020 to CE2065 is visible in the zonal means over almost all latitudes for most SRM techniques (Figure 6a). This increase is in all experiments strongest at polar northern latitudes which decreases the pole-to-equator temperature gradient and has implications for atmospheric dynamics: Meridional transport of heat is reduced, as well as the meridional
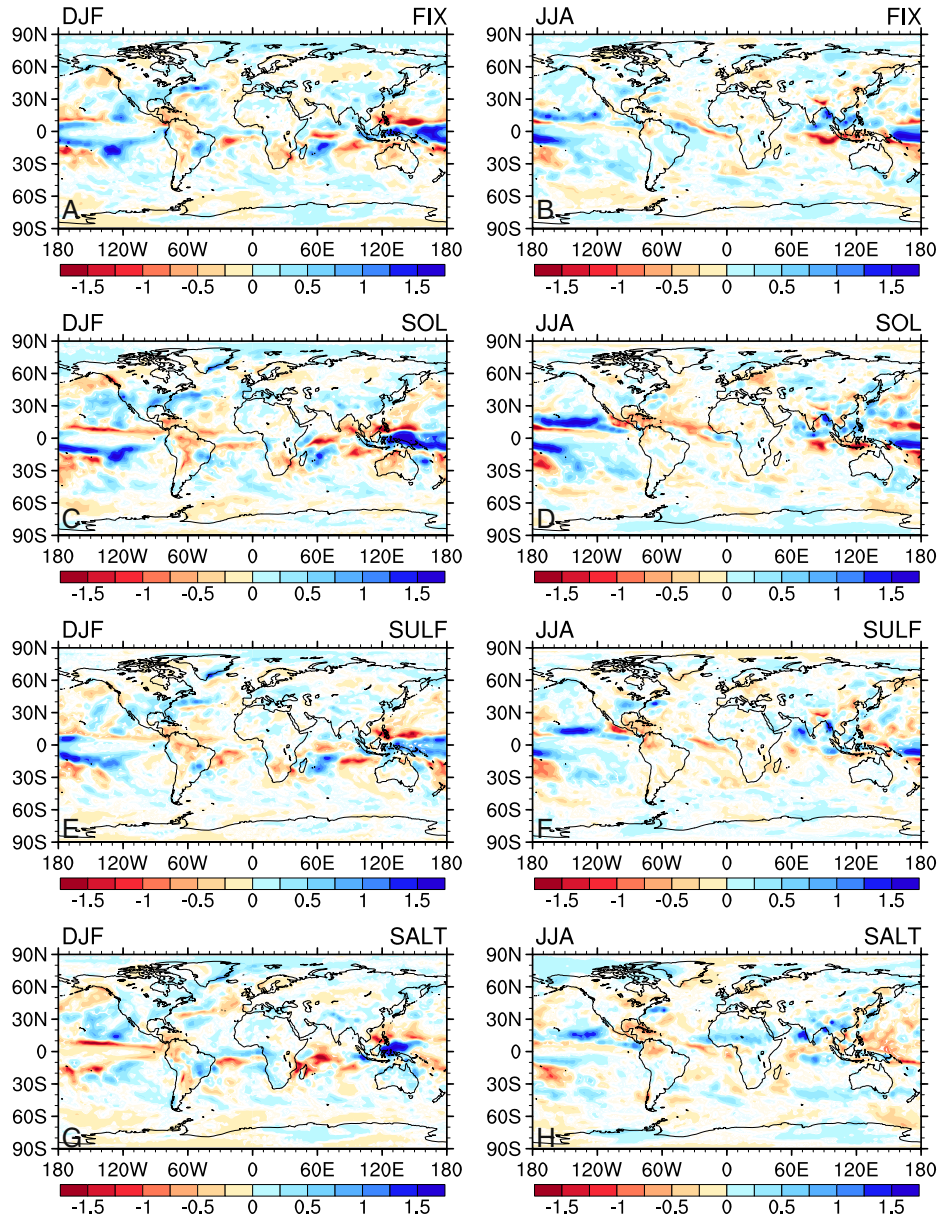
Figure 7. Seasonal precipitation anomaly (mm/d) of experiments (a and b) FIX, (c and d) SOL, (e and f) SULF, and (g and h) SALT for December-January-February (DJF) and June-July-August (JJA). Color-shaded areas are significant on 95% level. Anomalies are presented as differences between the engineered states CE2065 and the reference climate RCP2020.

extensions of the Hadley cell and the intertropical convergence zone (ITCZ). This causes precipitation increases near the equator, whereas arid areas with sinking air masses are shifted toward the equator (Figure 6b). Except for experiment SALT, changes in cloud cover are mostly related to changes in the ITCZ. The aerosol-based SRM experiments SULF and SALT show mainly a decrease of cloud cover (Figure 6d).

[44] As stated above, zonal mean responses in experiment SALT differ from the other experiments: Temperature, precipitation, and cloud cover changes have often an opposite sign than in the other experiments. The decrease in temperature in the tropics and increase over NH midlatitudes cause a stronger reduction of the temperature gradient between these areas than in the other experiments. As a consequence

of higher CDNC and smaller cloud droplets, precipitation decreases between 30°N and 30°S. We see in experiment SALT an increase in tropical cloud cover north of the equator. Cloud cover decreases in many parts of the Pacific south of the equator, with the only exception along the coast of Peru, caused by large-scale dynamical changes described in section 4.2 (see also K. Alterskjær et al. (submitted manuscript, 2013) for further details).

[45] Comparing the total zonal mean responses of FIX, SOL, and SULF to those over land surfaces only (Figures 6e–6h), some differences are evident, especially in the tropics: higher temperature, lower precipitation, lower extrema in the precipitation to evaporation difference (P-E), and increased ones for cloud cover over land. Higher land temperatures are owed to the lower heat capacity of land and
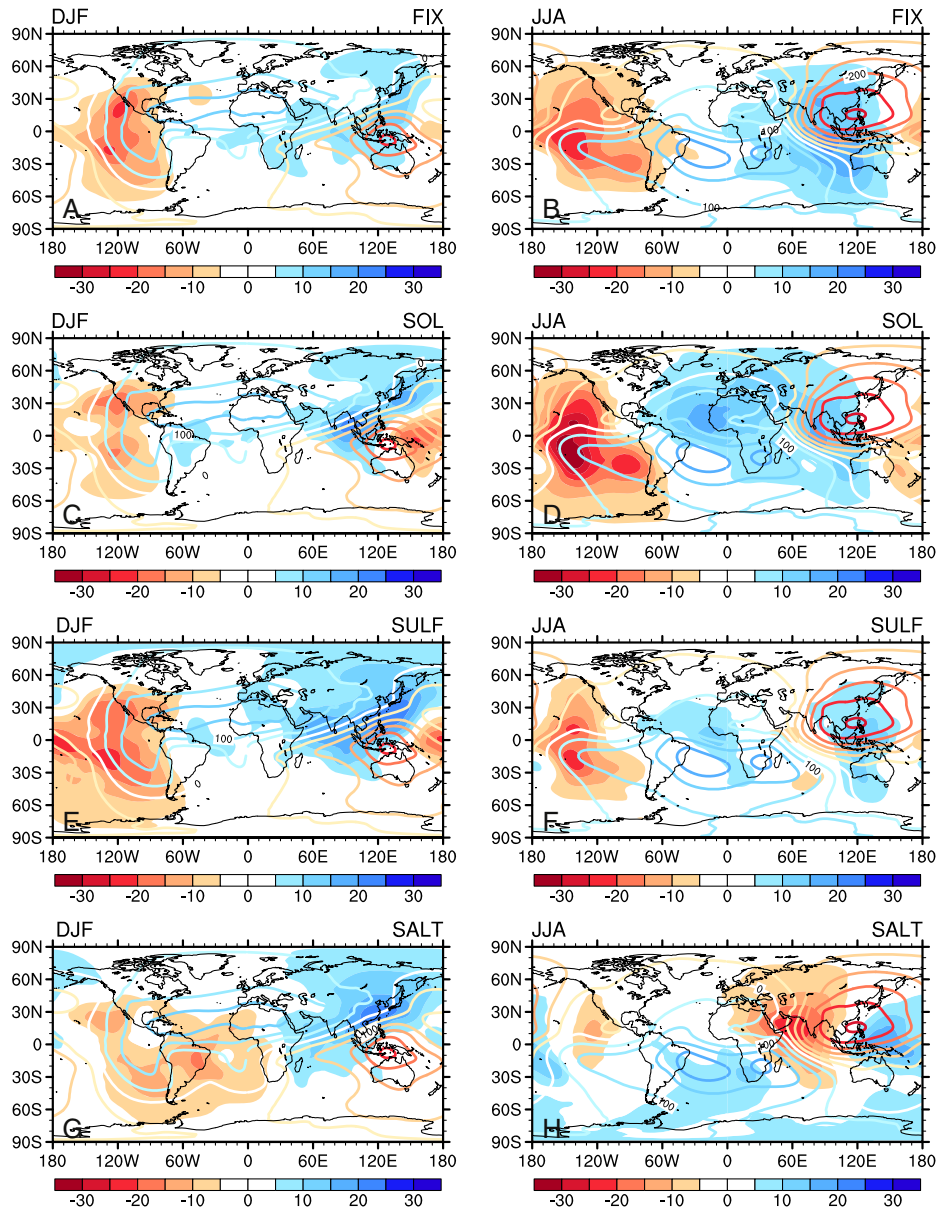
Figure 8. Velocity potential (m²/s) difference between the pressure levels of 200 and 850 hPa of experiments (a and b) FIX, (c and d) SOL, (e and f) SULF, and (g and h) SALT for DJF and JJA. Contour lines show the reference climate RCP2020, red represents ascending motion. Contour line colors are 10 times the values of the label bar. Shaded areas show differences of the last decade of the SRM experiments (CE2065) to RCP2020.

are further explained by *Joshi et al.* [2008] with feedbacks in the hydrological cycle, e.g., decreasing evaporation which is a cooling process.

[46] The relation between precipitation and evaporation (P-E) is a measure for water availability (Figures 6c and 6g). Over land decreasing evaporation in the tropics partly compensates the decrease in precipitation. Nevertheless, water availability decreases over tropical land areas as does cloud cover and precipitation. *Tilmes et al.* [2013] show the decrease in summer monsoon rain to be a robust feature in a multimodel ensemble of a SOL-type experiment (balancing 4 times CO_2 increase via reduction of solar constant). This can be related to shifts in the ITCZ and Walker circulations (see section 4.2).

4.2. Tropical Dynamics and Precipitation

[47] Precipitation in experiment SALT responds differently to the other SRM experiments: It increases over wide parts of tropical land areas, e.g., South-East Asia and Africa (Figures 6f, 7g, and 7h). SALT technique differs from the other methods because the precipitation release is directly influenced by the SRM through affecting the autoconversion. Additionally, the changes can be linked to large-scale dynamics: increasing vertical motion in the ascending branches of the ITCZ and Walker circulations and increasing precipitation (Figures 7g and 7h). This increase in deep convection precipitation compensates the decrease in precipitation from shallow clouds over the ocean. An analysis of the Southern Oscillation Index shows prevailing La Niña

conditions in SALT, even though El Niño events occur in single years (not shown).

[48] The difference of the seasonal mean of the velocity potential between 200 hPa and 800 hPa (Figure 8) emphasizes large-scale vertical motion, e.g., the Walker circulation in the tropics. Contour lines give RCP2020 conditions: ascending motion (red) over the west Pacific and Indian Ocean, descending motion over the east Pacific (blue) and Atlantic. The color-shaded areas are anomalies compared to RCP2020. They indicate for SALT (Figures 8g and 8h) a shift of the ascending area toward the Indian Ocean and Africa in NH summer (JJA), less pronounced in winter (DJF). Consequently, the descending area is extended from the eastern Pacific toward the central Pacific. These changes in the Walker circulation are partly comparable to the strengthened circulation during a La Niña event, visible in increasing and decreasing precipitation over Oceania in DJF and JJA, respectively (Figures 7g and 7h). Also, regionally, especially for Asia and Oceania, changes of precipitation patterns resemble the changes during La Niña conditions: Increase of precipitation over southern Africa, Brazil in DJF, and over India, southern China, and central Africa in JJA. These findings are similar to the results of *Nober et al.* [2003], who link similar changes in the velocity potential to emissions of anthropogenic aerosol. *Bala et al.* [2010] showed for sea salt seeding a similar enhancement of the monsoon, mainly over Asia, as presented in this study (Figure 6f). K. Alterskjær et al. (submitted manuscript, 2013) explain in detail the reasons for the increase in low-latitude cloud cover over land in SALT, comparing three different models.

[49] Almost opposite to SALT are the changes in the Walker circulation for FIX, SOL, and SULF (Figures 8a, 8c, and 8e). We see reduced vertical motion and a decrease of precipitation over the tropical Pacific, and an increase of descending motion over the Atlantic and Africa. Changes in precipitation patterns are mainly zonal as changes in the Hadley circulation dominate (Figures 7a–7f). This result agrees well with findings of *Bony et al.* [2013], linking the tendency toward El Niño conditions with the increase of CO_2.

[50] So far, this study is limited to one model. For a clear statement of impacts on regional scale, e.g., Amazonia, a comparison with a wider set of models is necessary, especially as tropical precipitation responses to temperature changes are not very robust among models [*Stevens and Bony*, 2013].

5. Summary and Conclusions

[51] We compared the climate impact of three different SRM techniques: Injection of sulfate into the stratosphere, mirrors in space, and artificial emissions of sea salt over the oceans. Simulations were performed following the GeoMIP G3 scenario where the increase of radiative forcing in the RCP4.5 scenario is balanced using stratospheric sulfate aerosol. The techniques were compared among each other and to a simulation where the radiative forcing was kept constant by simply fixing the GHG concentrations at 2020 levels. We mainly compared the differences between the engineered climates around 2065 and the reference climate of 2020.

[52] The main finding of our study is that the response of the hydrological cycle depends strongly on the applied SRM technique. It has been shown earlier based on theoretical considerations [*Bala et al.*, 2008] and in several modeling studies that the increase of precipitation resulting from the temperature increase in a GHG induced climate change would be overcompensated by an SRM forcing balancing the GHG forcing. This is confirmed for all SRM techniques of our study through the lower global mean precipitation compared to simulation FIX. This reduction, however, is about doubled for the aerosol-based techniques SALT and SULF in comparison to SOL. The quantitatively different effects of the SRM techniques can be explained with the atmospheric heating imbalance, the differences of the radiative budgets at surface and TOA. The differences among the techniques are influenced strongly by the absorption of LW radiation by both types of aerosols and the resulting greenhouse effect which requires a stronger reduction of net downward SW surface fluxes than in the case of space mirrors, and hence leads to a stronger reduction of the latent heat flux. Additionally, the height of the applied forcing and the regional distribution matters as the climate impact of globally applied forcing (SOL and SULF) differs from regional, ocean only forcing (SALT).

[53] A closer look on more regional impacts reveals that with respect to many climate variables, the responses to experiments SOL and SULF are similar to FIX. This similarity indicates that the response patterns are likely dominated by the temperature increase after 2020 caused by the residual radiative forcing. This may be different for larger amplitudes of SRM. Patterns of the responses to SALT differ in general more strongly in the seeding areas even for the relative small forcing applied here. The equator-to-pole temperature gradient, for instance, decreases in all experiments, showing the typical polar amplification patterns of global warming. Sea salt seeding, however, causes a much stronger reduction of the warming in the tropics, i.e., the region where the additional reflection of SW radiation is implemented.

[54] Not only the region of implementation but also the physical nature of this SRM technique differs from the others because the radiative properties are not only changed in clear sky due to increased sea salt loads. The clouds are manipulated directly by changing the CDNC over the oceans. This has an impact on the land/sea distribution of precipitation with decreasing precipitation over the oceans and increasing precipitation over land, similar to previous results on the impact of sea salt seeding [*Jones et al.*, 2010; *Bala et al.*, 2010; K. Alterskjær et al., submitted manuscript, 2013] and of an increase in tropospheric aerosols [*Nober et al.*, 2003]. Furthermore, our simulations indicate a change of the Walker circulation toward prevailing La Niña like conditions for sea salt emissions.

[55] Regional changes in precipitation between CE2065 and RCP2020 may reach ± 20% in yearly average over land, with the largest changes occurring in the tropics. The impact clearly depends on SRM technique and season.

[56] It should be noted that this study has some limitations: It was performed with a single model, the MPI-ESM, and the compensated RCP4.5 forcing is relatively small. Physical explanations given above increase our confidence that global mean differences in the response of the hydrological cycle among the SRM methods do not qualitatively

depend on the model. However, the robustness of regional responses should be studied using multimodel ensemble simulations. Unfortunately, in the original GeoMIP protocol [*Kravitz et al.*, 2011a], no directly comparable simulations for different SRM techniques are suggested. The multimodel intercomparison of GeoMIP G1 simulations by *Tilmes et al.* [2013] indicates that under such extreme forcings, many models show comparable responses of, e.g., precipitation responses in monsoon regions. Single model results in specific regions may nevertheless differ considerably. In the G3 setup, only the comparatively small RCP4.5 forcing after 2020 is compensated. Similar experiments for a stronger forcing may help to increase the signal-to-noise ratio of the results and thereby to better identify differences in particular in the regional responses to SRM techniques. We also limit this study to long-term averages. Changes in extreme values (see C. L. Curry et al. (A multi-model examination of climate extremes in an idealized geoengineering experiment, submitted to *Journal of Geophysical Research*, 2013) for such a study under the G1 experiment) or changes in daily temperature ranges seem also worth to be studied.

[57]   Balancing the transient increase of GHG to maintain the forcing of 2020 may sound like a not completely unrealistic approach, but it would impose many more problems in reality than in the model. Both the actual greenhouse gas forcing and the forcing of a certain amount of SRM can be estimated much more accurately in the model than in reality. Natural climate variability would pose a challenge for the rapid detection of SRM effects. It should also be mentioned that a potential abrupt ending of SRM would cause rapid climate change. *Jones et al.* [2013] calculated for the decade following the termination of SRM a global mean temperature increase of 2.4 K/decade in a multimodel ensemble of a 50 year SRM simulation balancing a 1%/year increase of CO_2. Finally, it needs to be repeated that important political, legal, and technical issues are related to SRM.

References

Albrecht, B. A. (1989), Aerosols, cloud microphysics, and fractional cloudiness, *Science*, 245, 1227–1230.

Alterskjær, K., J. E. Kristjánsson, and Ø. Seland (2012), Sensitivity to deliberate sea salt seeding of marine clouds observations and model simulations, *Atmos. Chem. Phys.*, 12, 2795–2807, doi:10.5194/acp-12-2795-2012.

Ammann, C., W. M. Washington, G. A. Meehl, L. Buja, and H. Teng (2010), Climate engineering through artificial enhancement of natural forcings: Magnitudes and implied consequences, *J. Geophys. Res.*, 115, D22109, doi:10.1029/2009JD012878.

Andrews, T., P. Forster, and J. Gregory (2009), A surface energy perspective on climate change, *J. Climate*, 22, 2557–2570, doi:10.1175/2008JCLI2759.1.

Bala, G., K. Caldeira, R. Nemani, L. Cao, G. Ban-Weiss, and H.-J. Shin (2010), Albedo enhancement of marine clouds to counteract global warming: Impacts on the hydrological cycle, *Clim. Dyn.*, 37, 915–931, doi:10.1007/s00382-010-0868-1.

Bala, G., P. B. Duffy, and K. E. Taylor (2008), Impact of geoengineering schemes on the global hydrological cycle, *Proc. Natl. Acad. Sci. USA*, 105, 7664–7669, doi:10.1073/pnas.0711648105.

Bentsen, M., et al. (2013), The Norwegian Earth System Model NorESM1-M, Part 1: Description and basic evaluation, *Geosci. Model. Dev.*, 6, 687–720.

Bony, S., G. Bellon, D. Klocke, S. Sherwood, and S. Denvil (2013), Robust direct effect of carbon dioxide on tropical circulation and regional precipitation, *Nat. Geosci.*, 6, 447–451, doi:10.1038/ngeo1799.

Budyko, M. I. (1977), *Climatic Changes*, 261 pp., American Geophysical Society, Washington, D.C. doi:10.1029/SP010.

Caldeira, K., and L. Wood (2012), Global and Arctic climate engineering: Numerical model studies, *Phil. Trans. R. Soc.*, 366, 4039–4056, doi:10.1098/rsta.2008.0132.

Crutzen, P. J. (2006), Albedo enhancement by stratospheric sulfur injections: A contribution to resolve a policy dilemma?, *Clim. Change*, 77, 211–219.

Giorgetta, M., et al. (2013), Climate and carbon cycle changes from 1850 to 2100 in MPI-ESM simulations for the coupled model intercomparison project phase 5, *J. Adv. Model. Earth Syst.*, 5, doi:10.1002/jame.20038.

Giorgetta, M. A., E. Manzini, E. Roeckner, M. Esch, and L. Bengtsson (2006), Climatology and forcing of the quasi-biennial oscillation in the MAECHAM 5 model, *J. Climate*, 19, 3882–3901.

Govindasamy, B., and K. Caldeira (2000), Geoengineering Earth's radiation balance to mitigate climate change, *Geophys. Res. Lett.*, 27, 2141–2144.

Gregory, J. M., W. J. Ingram, M. A. Palmer, G. S. Jones, P. A. Stott, R. B. Thorpe, J. A. Lowe, T. C. Johns, and K. D. Williams (2004), A new method for diagnosing radiative forcing and climate sensitivity, *Geophys. Res. Lett.*, 31, L03205, doi:10.1029/2003GL018747.

Hansen, J., et al. (2005), Efficacy of climate forcings, *J. Geophys. Res.*, 110, D18104, doi:10.1029/2005JD005776.

Hansen, J., M. Sato, and R. Ruedy (1997), Radiative forcing and climate response, *J. Geophys. Res.*, 102, 6831–6864, doi:10.1029/96JD03436.

Irvine, P. J., A. Ridgwell, and D. J. Lunt (2011), Climatic effects of surface albedo geoengineering, *J. Geophys. Res.*, 116, D24112, doi:10.1029/2011JD016281.

Jones, A., J. Haywood, and O. Boucher (2009), Climate impacts of geoengineering marine stratocumulus clouds, *J. Geophys. Res.*, 114, D1010, doi:10.1029/2008JD011450.

Jones, A., J. Haywood, and O. Boucher (2011), A comparison of the climate impacts of geoengineering by stratospheric SO_2 injection and by brightening of marine stratocumulus cloud, *Atmos. Sci. Lett.*, 12, 176–183, doi:10.1002/asl.291.

Jones, A., et al. (2013), The 'termination effect' in experiment G2 of the Geoengineering Model Intercomparison Project (GeoMIP), *J. Geophys. Res. Atmos.*, 118, 9743–9752, doi:10.1002/jgrd.5076.

Jones, A., J. Haywood, O. Boucher, B. Kravitz, and A. Robock (2010), Geoengineering by stratospheric SO_2 injection: Results from the Met Office HadGEM2 climate model and comparison with the Goddard Institute for Space Studies ModelE, *Atmos. Chem. Phys.*, 10, 5999–6006, doi:10.5194/acp-10-5999-2010.

Joshi, M., J. G. M. Webb, D. Sexton, and T. Johns (2008), Mechanisms for the land/sea warming contrast exhibited by simulations of climate change, *Clim Dyn*, 30, 455–465, doi:10.1007/s00382-007-0306-1.

Jungclaus, J., N. Fischer, H. Haak, K. Lohmann, J. Marotzke, D. Matei, U. Mikolajewicz, D. Notz, and J. von Storch (2013), Characteristics of the ocean simulation in MPIOM, the ocean component of the MPI-Earth System Model, *J. Adv. Model. Earth Syst.*, 2, 117–458, doi:10.1002/jame.20032.

Kravitz, B., A. Robock, O. Boucher, H. Schmidt, K. E. Taylor, G. Stenchikov, and M. Schulz (2011a), The Geoengineering Model Intercomparison Project (GeoMIP), *Atmos. Sci. Lett.*, 12, 162–167, doi:10.1002/asl.316.

Kravitz, B., A. Robock, O. Boucher, H. Schmidt, and K. E. Taylor (2011b), Specifications for GeoMIP experiments G1 through G4. http://climate.envsci.rutgers.edu/GeoMIP/publications.html.

Kravitz, B., et al. (2013b), Climate model response from the Geoengineering Model Intercomparison Project (GeoMIP), *J. Geophys. Res. Atmos.*, 118, 8320–8332, doi:10.1002/jgrd.50646.

Latham, J. (1990), Control of global warming?, *Nature*, 347, 339–340.

Lenton, T. M., and N. E. Vaughan (2009), The radiative forcing potential of different climate engineering options, *Atmos. Chem. Phys.*, 9, 5539–5561.

Li, J., X. Ma, K. von Salzen, and S. Dobbie (2008), Parameterization of sea-salt optical properties and physics of the associated radiative forcing, *Atmos. Chem. Phys.*, 8, 4787–4798, www.atmos-chem-phys.net/8/4787/2008/.

Liepert, B. G., and M. Previdi (2009), Do models and observations disagree on the rainfall response to global warming?, *J. Climate*, *22*, 3156–3166, doi:10.1175/2008JCLI2472.1.

Lohmann, U., and J. Feichter (2005), Global indirect aerosol effects: A review, *Atmos. Chem. Phys.*, *5*, 715–737, doi:10.5194/acp-5-715-2005.

Mautner, M. (1991), A space-based solar screen against climate warming, *J. Brit. Interpl. Soc.*, *44*, 135–138.

Niemeier, U., H. Schmidt, and C. Timmreck (2011), The dependency of geoengineered sulfate aerosol on the emission strategy, *Atmos. Sci. Let.*, *12*, 189–194, doi:10.1002/asl.304.

Nober, F., H. Graf, and D. Rosenfeld (2003), Sensitivity of the global circulation to the suppression of precipitation by anthropogenic aerosols, *Global Planet. Change*, *37*, 57–80, doi:10.1016/S0921-8181(02)00191-1.

Partanen, A.-I., H. Kokkola, S. R. M. V.-M. Kerminen, K. E. J. Lehtinen, T. Bergman, A. Arola, and H. Korhonen (2012), Direct and indirect effects of sea spray geoengineering and the role of injected particle size, *J. Geophys. Res.*, *117*, D02203, doi:10.1029/2011JD016428.

Rasch, P. J., P. J. Crutzen, and D. B. Coleman (2008), Exploring the geoengineering of climate using stratospheric sulfate aerosols: The role of particle size, *Geophys. Res. Lett.*, *35*, L02809, doi:10.1029/2007GL032179.

Reick, C., T. Raddatz, V. Brovkin, and V. Gayler (2013), The representation of natural and anthropogenic land cover change in MPI-ESM, *J. Adv. Model. Earth Syst.*, *5*, doi:10.1002/jame.20022.

Ricke, K. L., M. G. Morgan, and M. R. Allen (2010), Regional climate response to solar-radiation management, *Nat. Geosci.*, *3*, 537–541, doi:10.1038/ngeo915.

Robock, A., L. Oman, and G. L. Stenchikov (2008), Regional climate responses to geoengineering with tropical and Arctic SO_2 injections, *J. Geophys. Res.*, *113*, D16101, doi:10.1029/2008JD010.

Rosenfeld, D., U. Lohmann, G. B. Raga, C. D. O'Dowd, M. Kulmala, S. Fuzzi, A. Reissell, and M. O. Andreae (2008), Flood or drought: How do aerosols affect precipitation?, *Science*, *321*(5894), 1309–1313, doi:10.1126/science.1160606.

Schmidt, H., et al. (2012), Solar irradiance reduction to counteract radiative forcing from a quadrupling of CO_2: Climate responses simulated by four Earth system models, *Earth Syst. Dyn.*, *3*(1), 63–78, doi:10.5194/esd-3-63-2012.

Stevens, B., and S. Bony (2013), What are climate models missing?, *Science*, *340*(6136), 1053–1054, doi:10.1126/science.1237554.

Stevens, B., et al. (2013), The atmospheric component of the MPI-M Earth System Model: ECHAM6, *J. Adv. Model. Earth Syst.*, *5*, 1–27, doi:10.1002/jame.20015.

Stier, P., et al. (2005), The aerosol-climate model ECHAM5-HAM, *Atmos. Chem. Phys.*, *5*, 1125–1156.

Struthers, H., A. M. L. Ekman, P. Glantz, T. Iversen, A. Kirkevåg, E. Mårtensson, O. Seland, and E. D. Nilsson (2011), The effect of sea ice loss on sea salt aerosol concentrations and the radiative balance in the Arctic, *Atmos. Chem. Phys*, *11*, 3459–3477, doi:10.5194/acp-11-3459-2011.

Taylor, K. E., R. J. Stouffer, and G. A. Meehl (2012), An overview of CMIP5 and the experiment design, *Bull. Amer. Meteor. Soc.*, *93*, 485–498, doi:10.1175/BAMS-D-11-00094.1.

Tilmes, S., et al. (2013), The hydrologic impact of geoengineering in the Geoengineering Model Intercomparison Project (GeoMIP), *J. Geophys. Res. Atmos.*, doi:10.1002/jgrd.50868.

Timmreck, C., H.-F. Graf, S. J. Lorenz, U. Niemeier, D. Zanchettin, D. Matei, J. H. Jungclaus, and T. J. Crowley (2010), Aerosol size confines climate response to volcanic super-eruptions, *Geophys. Res. Lett.*, *37*, L2470, doi:10.1029/2010GL045464.

Trenberth, K., and A. Dai (2007), Effects of Mount Pinatubo volcanic eruption on the hydrological cycle as an analog of geoengineering, *Geophys. Res. Lett.*, *34*, L15702, doi:10.1029/2007GL030524.

Twomey, S. (1977), Influence of pollution on shortwave albedo of clouds, *J Atmos Sci*, *34*, 1149–1152, doi:10.1175/1520-0469(1977)034<1149:TIOPOT>2.0.CO;2.